Journal of Alloys and Compounds 750 (2018) 17–22

Contents lists available at ScienceDirect

Journal of Alloys and Compounds

journal homepage: http://www.elsevier.com/locate/jalcom

The origin of cycling enhanced capacity of Ni/NiO species confined on nitrogen doped carbon nanotubes for lithium-ion battery anodes

Yidong Luo [a, 1], Mouyi Weng [b, 1], Jiaxin Zheng [b], Qinghua Zhang [a], Bingqing Xu [a], Shaoqing Song [c], Yang Shen [a], Yuanhua Lin [a, *], Feng Pan [b, **], Cewen Nan [a]

[a] State Key Laboratory of New Ceramics and Fine Processing, School of Materials Science and Engineering, Tsinghua University, Beijing 100084, PR China
[b] School of Advanced Materials, Shenzhen Graduate School, Peking University, Shenzhen 518055, PR China
[c] Key Laboratory for Radioactive Geology and Exploration Technology, Fundamental Science for National Defense, East China University of Technology, Nanchang, 330013, PR China

ARTICLE INFO

Article history:
Received 30 November 2017
Received in revised form
7 March 2018
Accepted 21 March 2018
Available online 23 March 2018

Keywords:
Confinement effect
Lithium ion battery
Core-shell nanostructure

ABSTRACT

We demonstrate that the confinement effect of the NiO compound can directly enhance the electrochemical performance upon cycling. Fabricating the core-shell C-coated Ni/NiO nanofibers (e.g., Ni and NiO, nitrogen doped carbon respectively) composite electrode largely increases the capacity (1332 mAh g^{-1} vs 718 mA h g^{-1}) and improve the long-term cycling stability. The High Angle Annular Dark Field results reveal that the doped pyridine-like nitrogen shell will divide the NiO into smaller nanoparticle during the charging and discharging process. In addition, the density functional theory calculation suggests the confined nanoscale NiO(Ni) will absorb and react with Li ions more easily. With cycling, smaller NiO/Ni nanoparticle will bring more active sites, leading additional interfacial lithiation capacity. At the same time, the confinement effect of the NiO compound further increases the capacity of the nanocomposites.

1. Introduction

Li ion battery has been intensively utilized in portable electronics and show significant promise for applications [1–3]. The energy density and cycling performance of lithium ion batteries depend on the physical and chemical properties of both cathode and anode materials. Transitional metal oxides, such as NiO based nanomaterials have attracted considerable attention as potential substitutes for graphite because of their numerous appealing features, including abundance, low cost, environmental benignity, and high theoretical capacity [4–7]. Nanostructured coating can restrain the volumetric change in the electrode and prevent the aggregation of the active materials which can enhance the cycling stability of batteries [8–12]. For lithium ion anode materials, an effective implementation of this concept is to use a multilayer thin film structure comprised of Si (or other high capacity materials) and inert metal layers (e.g., Ti, Al, and Zn) [10,13–15]. Studies of Si-based multilayer electrodes show strong differences in reversible capacity and cycling stability as a function of the thicknesses of the buffer and active layers. The technical challenges of Li-alloying reactions (e.g., with Si) are similar to those found in the conversion reactions of metal oxides electrodes [10,15]. As for the NiO, study results [16] show that the lithiation of NiO involve the formation and decomposition of Li_2O, with the reduction and oxidation of metal nano-particles in the range of 5–10 nm in diameter. In particular, nanoscale confinement of nanosized metal oxide particles is believed to improve the lithiation and delithiation electrochemical performance.

In order to explore the critical role of nanoscale confinement effect in electrochemical process of the formation/decomposition of Li_2O, we design a core-shell C-coated Ni/NiO nanofibers composite electrode. In particular, NiO is a promising anode material for LIBs due to its high theoretical specific capacity (718 mA h g^{-1}), abundant material supply and low cost. As NiO has low electronic conductivity, it is always composited with conductive materials. These composite anodes exhibited high reversible capacity and excellent electrochemical performance. However, the capacity of NiO based anode usually shows a decrease during lithiation and

* Corresponding author.
** Corresponding author.
E-mail addresses: linyh@mail.tsinghua.edu.cn (Y. Lin), panfeng@pkusz.edu.cn (F. Pan).
[1] These authors contributed equally to this work.

https://doi.org/10.1016/j.jallcom.2018.03.269
0925-8388/

delithiation process due to the formation of the SEI layer [16–22]. Interestingly, the increase in cycling induced capacity has been found in the NiO and other metal oxide electrodes upon long cycles. These phenomena may partly attribute to the activation of the conductive materials. Its origin arouses much attention and much effort has been devoted to the search. Nevertheless, the reason for the increased capacity with the cycling still remains unclear. One of the possible reasons is the lack of an effective model which can explain the activation mechanism based on experiment and calculation results. On the other hand, NiO based anodes are usually composited with other additives, increasing the difficulty to identify the confinement effect in electrochemical process.

Here, we design a core-shell C-coated Ni/NiO nanofibers composite electrode by employing the electrospinning and Chemical Vapor Deposition (CVD) methods. With the N-doped carbon coating, the core–shell C-coated Ni/NiO nanofibers exhibits remarkable reversible capacity and capacity retention. The formed nano reactor between the inner cavity of C-coated layer and NiO excludes other factor caused by the outside additives, and give an isolated space to explore the activation mechanism. The results find the nano reactor can facilitate effective lithiation and delithiation processes as well as NiO/Ni redox by confinement effect. In addition, the density functional theory calculation suggests that the confined NiO(Ni) can absorb and react with Li ions more easily.

2. Experimental

2.1. Synthesis of C-coated Ni/NiO nanofibers

Firstly, C-coated Ni/NiO nanofibers electrocatalysts were fabricated by electrospinning-chemical vapor deposition method. In detail, 0.8 g PVP and 0.45 g $Ni(AC)_2 \cdot 4H_2O$ were dissolved in 10 mL ethanol and then magnetically stirred at room temperature for 12 h. Afterwards, the resulting homogeneous mixture was loaded into a spinneret which was linked to a high-voltage equipment with 15 KV working voltage. Aluminum foil was used as collector to gain the spinning sample at the rate of 2 ml h^{-1} by syringe pump in the relative humidity of 30%, and the primary spinning sample was heated at 660 °C for 2 h at rate of 2 °C/min in a furnace. After the heating treatment, sample was grinded and then placed on horizontal quartz tube of furnace. The furnace reaction chamber was evacuated and flushed with N_2 for several times to remove oxygen and moisture, then the reactor was heated to 800 °C at a rate of 10 °C/min in N_2. 10 mL pyridine as precursor was injected into the reaction chamber for about 30 min by N_2. After the CVD reaction, a dark sponge-like product was obtained and labeled as C-coated Ni/NiO nanofibers.

2.2. Characterization

The morphology was observed with using field emission scanning electron microscopy (FE-SEM; JEOL JSM-7001F) and high-resolution transmission electron microscopy (HRTEM, JEOL2011). The chemical component was investigated by X-ray diffraction (XRD, Rigaku D/max-2500 instrument using Cu Kα radiation (40 kV) with a scanning rate of 0.067°/s). The chemical state was performed with X-ray photoelectron spectroscopy (XPS, ultra-high-vacuum ESCALAB 250Xi electron spectrometer). The binding energies of XPS spectra refer to C 1s at 284.6 eV. Raman spectra were conducted on an INVIA spectrophotometer (Renishaw, UK).

2.3. Electrochemical test

CR2032 coin type half cells were fabricated in an argon-filled glovebox with Li metal as the counter electrode. 1 M $LiPF_6$ in ethyl carbonate/dimethyl carbonate (1:1 by volume) was used as electrolyte, and a porous polypropylene film (Celgard 2400, Celgard Inc., USA) was used to separate the two electrodes. Charge/discharge tests were conducted at different current densities in a potential range of 0.01~3 V vs. Li/Li^+ with a battery test system (C2001A, LAND, China). Cyclic voltammograms (CV) measurements were carried out at a scan rate of 0.1 mV s^{-1} between 0.01 and 3 V using CHI760 Battery Tester.

2.4. Calculation method

The DFT calculations were performed by using the Vienna Ab-initio Simulation Package (VASP) [23] using local-density approximation (LDA) exchange-correlation functional with Projector augmented-wave method (PAW) [24–26]. The cut-off energy is set to be 450 eV and a k-points mesh is set to be $6 \times 6 \times 1$ including gamma point. During the geometry optimizations, the lattice constants were fixed. A vacuum buffer space of 20 Å is set above lithium atoms. The lithium atom adsorption was calculated on a six-layer 2×2 nickel (111) slab. For each ratio, we calculated two or three possible arrangement of lithium atom on the surface.

3. Results and discussion

3.1. Structure and morphology of the C-coated Ni/NiO nanofibers

The XRD patterns of NiO nanofibers and C-coated Ni/NiO nanofibers are shown in Fig. 1a. It is seen that peaks for the two samples at $\theta = 37.2°$, 43.4°, 62.9°, 75.2° and 79.4°should be assigned well to (111), (200), (220), (311) and (222) diffraction of NiO (JCPDS 65-6920). After CVD treatment, new diffraction peaks for C-coated Ni/NiO nanofibers can be seen at 44.2°, 51.6°, and 76.1° corresponding to (111), (200), and (220) of Ni (JCPDS 65-0380), respectively. Moreover, the intensity of NiO diffraction peaks was reduced over C-coated Ni/NiO nanofibers due to the existence of Ni, indicating partial NiO was reduced into Ni in the process of carbon coating by the CVD treatment. The XRD diffraction peaks for carbon layers can be probed at 21.2°, 30.3°, 31.6°, 76.1°, which may be attributed to the produced C-coated layer. Raman spectroscopy is often used to investigate the production and its graphitization structure of carbon nano materials. As seen in Fig. 1b C-coated Ni/NiO nanofibers sample presents two primary peaks at 1342 and 1576 cm^{-1} corresponding to the vibrations of carbon atoms in the disordered graphite structure (i.e., defects, named D band) and the E_{2g} mode of graphite (i.e., graphite structure, named G band), and thus the intensity ratio of G band to D band (I_G/I_D) presents the graphitization degree. In Fig. 1b, we can see that I_G/I_D is about 0.6, indicating the existence of poor graphite structure for C-coated Ni/NiO nanofibers.

To further investigate the surface composition of NiO nanofiber and C-coated Ni/NiO nanofibers, the XPS spectra (Fig. 1c) of Ni 2p for the two samples distributes the regions of 850–857.5 eV and 857.5–866 eV, corresponding to Ni 2p3/2 and satellite peak. The Ni 2p3/2 peak of two samples can be deconvoluted into two components centered at 871.8 and 874.89 eV, ascribable to the characteristic of Ni^{2+} and Ni species, respectively. A quantitative analysis based on the integrated area of two decomposed peaks could give rise to the relative proportion of Ni to Ni^{2+} species. The molar ratio of Ni/Ni^{2+} is 1.6:1 and 1:2.4 for NiO nanofiber and C-coated Ni/NiO nanofibers, suggesting the existence of Ni after coating.

Fig. 2a presents the morphologies and structures of the samples examined by TEM. We can see that NiO nanofiber was coated with carbon. Moreover, NiO nanofiber with length of 600–800 nm were continuous dispersed in the C-coated layer, thus the formed nano reactor between the inner cavity of C-coated layer and NiO is

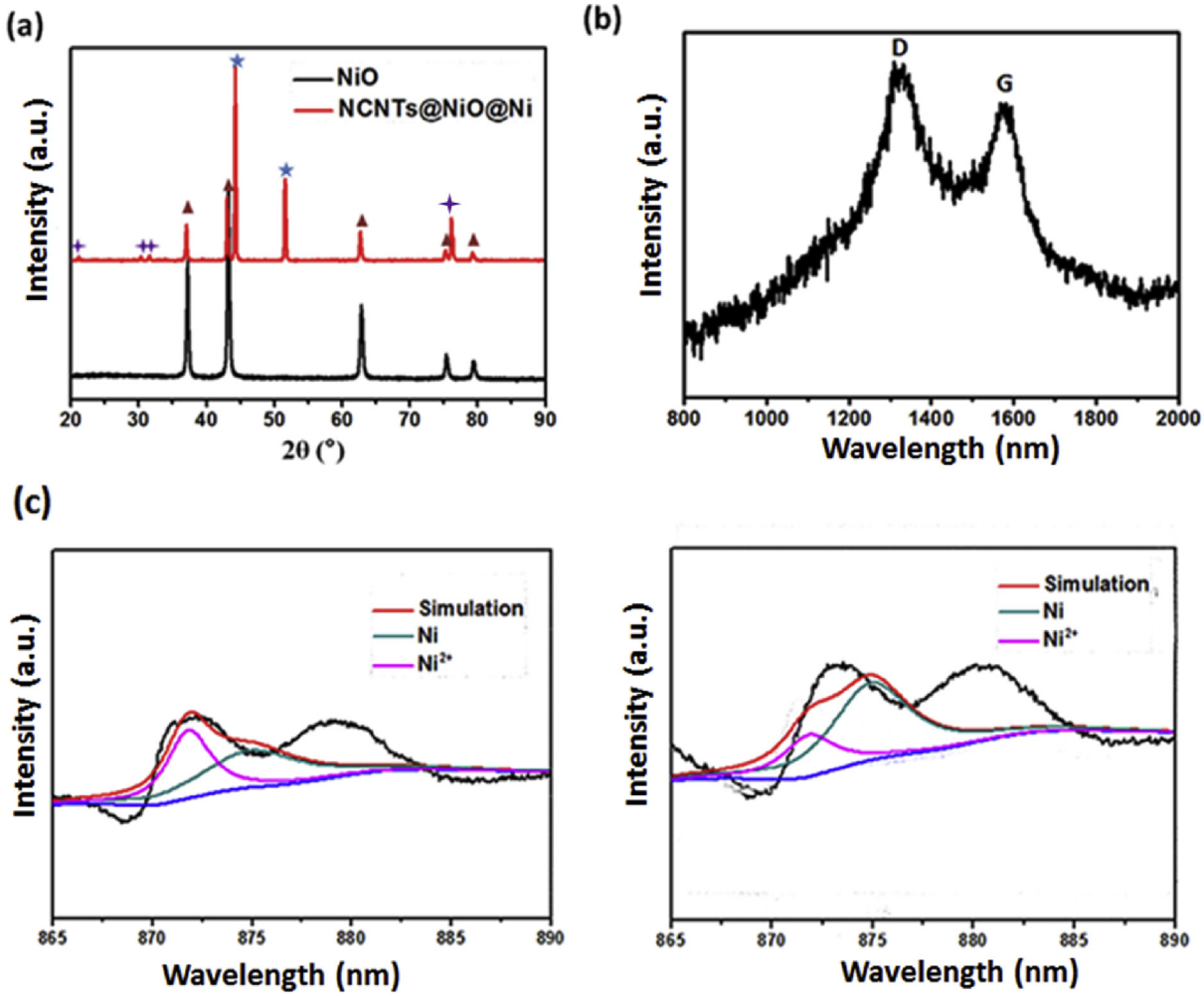

Fig. 1. (a) XRD patterns and (b) Raman spectra of C-coated Ni/NiO nanofibers array; (c) XPS spectra of NiO@Ni before and after coating (left and right).

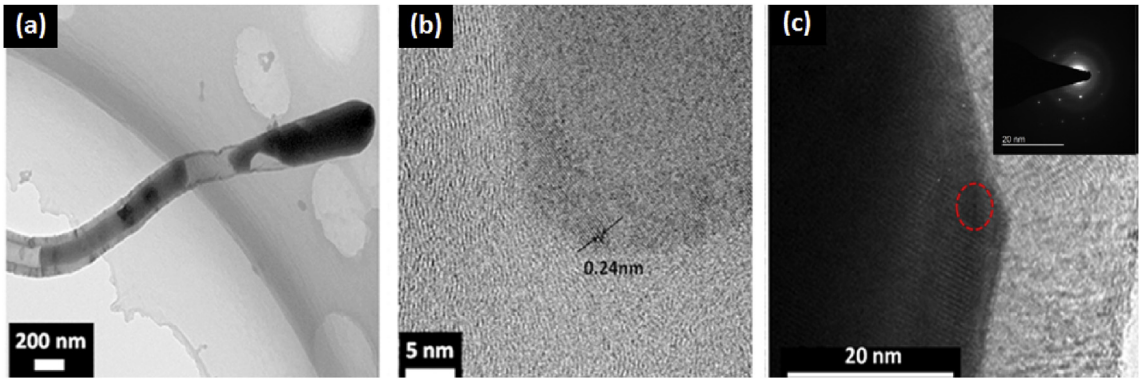

Fig. 2. (a) A TEM image of C-coated Ni/NiO nanofibers; (b), (c) HRTEM image of C-coated Ni/NiO nanofibers; Inset : SAED of C-coated Ni/NiO nanofibers.

beneficial to lithiation and delithiation processes as well as NiO/Ni redox by confinement effect. In Fig. 2b, the lattice fringes with a spacing of 0.24 nm were observed in the C-coated Ni/NiO nanofibers, corresponding to the (111) plane of NiO. The ring-like mode in the selected-area electron diffraction (SAED) pattern can confirm the NiO species in the C-coated Ni/NiO nanofibers.

3.2. Electrochemical performance

The electrochemical activity of the prepared anode electrodes was firstly tested at a 200 mA g^{-1} in Fig. 3a. NiO nanofiber electrode can only achieve an initial charge capacity of 743 mAh g^{-1}, and the charge capacity continuously decreases with cycling, and drop to 383 mAh g^{-1} after 40^{th} cycle because of the growth of SEI film, with

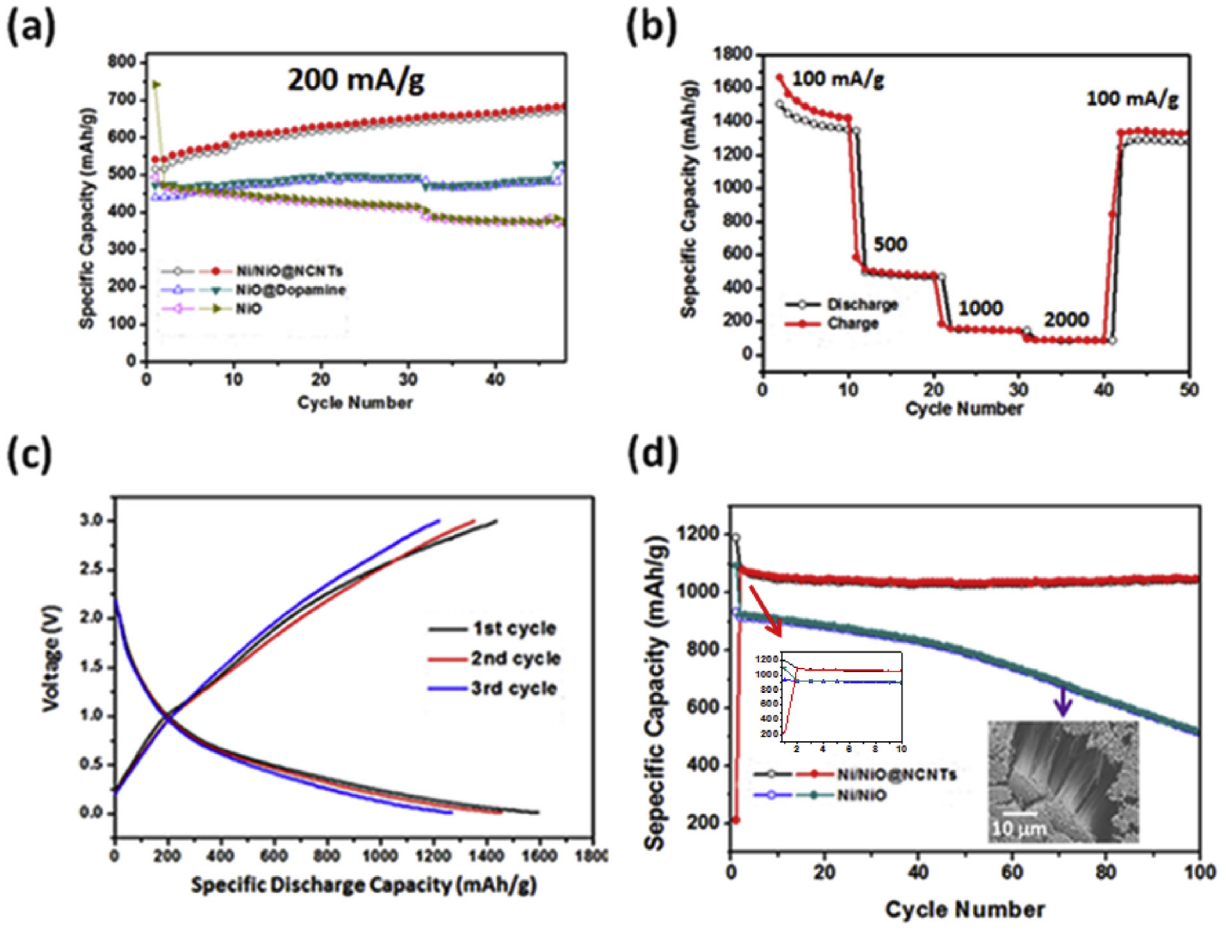

Fig. 3. (a) Cycling performance at 200 mA g^{-1} of C-coated Ni/NiO nanofibers, NiO@Dopamine, NiO; (b) Rate performance of C-coated Ni/NiO nanofibers at different current densities from 0.1 to 2 A g^{-1} (Hollow: discharge; solid: charge); (c) Charge-discharge curves of C-coated Ni/NiO nanofibers at 100 mA g^{-1}; (d) Cycling performance at 200 mA g^{-1} of C-coated Ni/NiO nanofibers array. Inset: SEM images of the Ni@NiO arrays.

the charge capacity efficiency reduced by 52%. Nevertheless, initial charge capacity of C-coated Ni/NiO nanofibers electrode can reach at 545 mAh g^{-1}, moreover, the charge capacity efficiency continuously increases by 22.4%, and reached 667 mAh g^{-1} after 40th cycle. Combined with Figs. 1 and 2, we can see the electrocatalytic activity of C-coated Ni/NiO nanofibers was enhanced by the improved composites, morphology, and electronic characteristics by coating with carbon layer. In Fig. 3b, the reversible capacities of C-coated Ni/NiO nanofibers can reach to 1662 mAh g^{-1} at a current density of 0.1 A g^{-1}. As the current densities varied from 0.1 to 2 A g^{-1}, the specific capacity can be recovered to 1332 mAh g^{-1}, which C-coated Ni/NiO nanofibers presents good charge-discharge capability. Fig. 3c shows the potential versus capacity profiles of C-coated Ni/NiO nanofibers during the 1st, 2nd, and 3rd cycles at 100 mA g^{-1}. The charging/discharging profiles of C-coated Ni/NiO nanofibers are similar in the cycles process. The first discharging capacity of C-coated Ni/NiO nanofibers is 1600 mAh g^{-1}, which is much higher than the previous reported electrocatalysts. Moreover, the potentials of C-coated Ni/NiO nanofibers at approximately 1.0 V in these cycles, indicate the highly efficient conversion between NiO and Ni ($NiO + 2Li \Leftrightarrow Li_2O + Ni$) due to the confinement effect of C-coated layer.

To verify the assumption, Ni/NiO was fabricated according to pulsed laser deposition and used as the cathode in the charge and discharge test of lithium battery. The recycle electrocatalytic performances of Ni/NiO and C-coated Ni/NiO nanofibers were shown in Fig. 3d at 200 mA rate. The first discharge capacity over Ni/NiO reached to 1092 mAh g^{-1}, however, the capacity for Ni/NiO decreased to 907 mAh g^{-1} in the second recycle. More positively, compared with Ni/NiO electrocatalyst, C-coated Ni/NiO nanofibers shows a higher reversible electrocapacity and retention. In Fig. 3d, it can be seen that the electrocatalytic capacity over C-coated Ni/NiO nanofibers increased to 1046 mAh g^{-1} after 100 cycles. Therefore, C-coated Ni/NiO nanofibers presents high electrocatalytic activity and stability due to the confinement effect of C-coated layer on the redox of NiO/Ni as well as the adsorption and insertion of lithium ion in the charge and discharge process of lithium battery.

In order to confirm effective redox capability between NiO to Ni with the aid of C-coated layer confinement effect, the morphology and composition of C-coated Ni/NiO nanofibers were investigated after charge-discharge recycle. The HAADF result shows that, compared with the size before lithiation, Ni/NiO NPs were smaller with the size of 5–180 nm, as illustrated in Fig. 4a, and the corresponding TEM and HRTEM show that Ni/NiO species diffused into nano layer of C-coated layer, as confirmed by EDS characterization [27]. Moreover, we investigated the adsorption behavior of Li^+ on Ni (111) crystal surface by calculating binding energy between Li atoms and nickel clusters. In Fig. 5, it is seen that the binding energy is −1.37eV when the ratio of Li^+/Ni is 0.25, indicating Li ions were preferentially adsorbed on the surface of Ni. Furthermore, the binding energy remain negative when increasing the ratio of Li^+/Ni

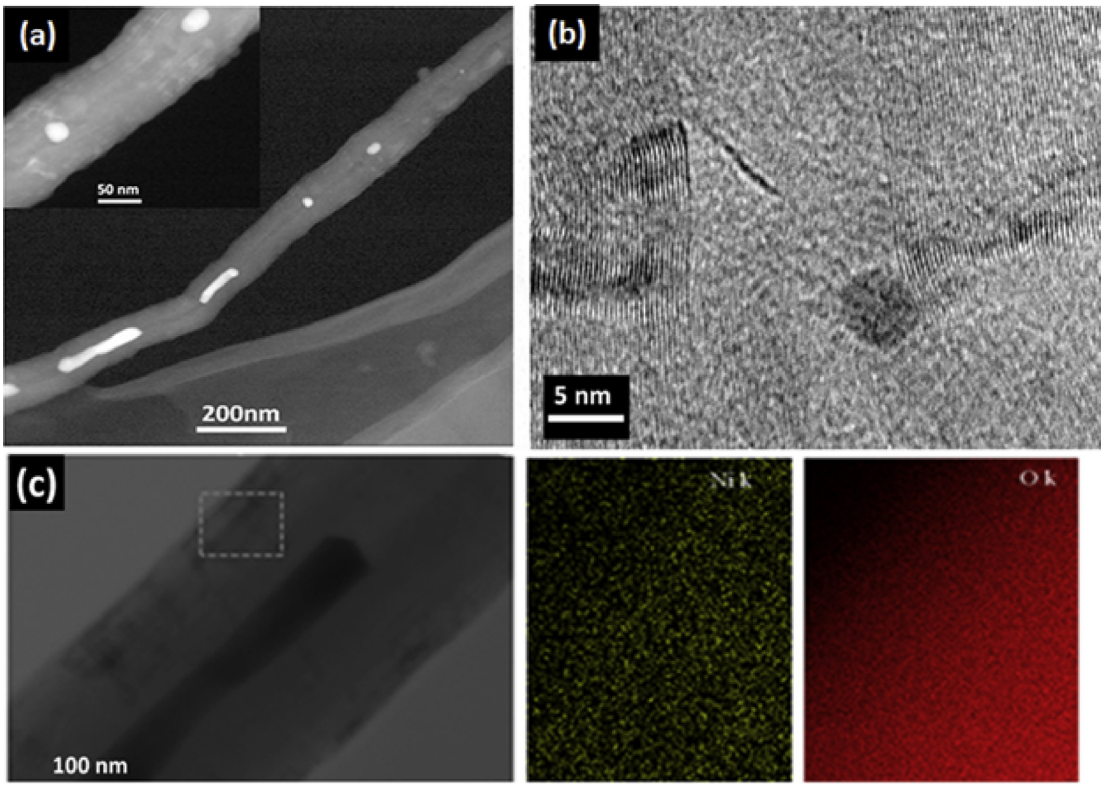

Fig. 4. (a) HAADF images of the C-coated Ni/NiO nanofibers after the lithiation; (b) TEM images of the C-coated Ni/NiO nanofibers after the lithiation; (c) TEM image and the EDS elemental mapping of the C-coated layer@NiO@Ni.

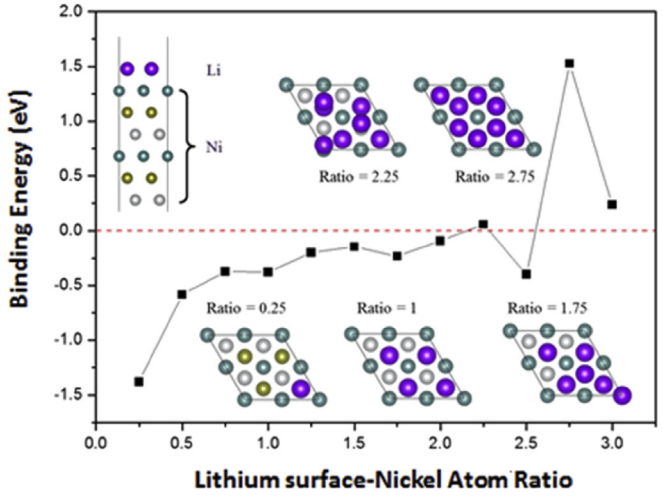

Fig. 5. Binding energy with different lithium surface-nickel atom ratios. The inset figures indicate configurations of different lithium atom numbers. Different nickel atoms are in different colors according to their positions. (For interpretation of the references to color in this figure legend, the reader is referred to the Web version of this article.)

from 0.25 to 2.5. When the ratio of Li^+/Ni increased to 2.75, the binding energy shows the positive value, suggesting the accumulated Li ions enhance the adsorption energy barrier. The calculation results show that the nano scale Ni/NiO can store 25 percent Li more than theoretical value. On the other hand, the result indicates the reaction of Li_2O to Li_2O_2. Usually, the reaction of Li_2O to Li_2O_2 does not happen because the highly insulating Li_2O_2 can automatically shut down the reaction [28]. However the smaller NiO particle upon the cycling may acts as catalyst in such a reaction. Therefore, the smaller NiO particles provide more active surface area and may act as catalyst in the reaction of Li_2O to Li_2O_2.

4. Conclusions

In summary, the C-coated Ni/NiO nanofibers were prepared by a simple electrospinning approach followed by CVD reaction. The specific combination of composition shows superior features with a specific discharge capacity of 1662 mA g^{-1} at a current density of 0.1 A g^{-1}. Experimental evidence confirm the N-doping brings multifold revolutionary effects on the Li storage of Ni/NiO hybrid composite electrodes. The increasing active sites of NiO serves as a major contributor to the enhanced capacity upon long cycling. The confinement effect of the nano scale NiO effectively enhancing the electrochemical performance and showed a better characteristic in storing lithium. Our finding will shed new light on understanding of oxide conversion reactions in lithium ion batteries, guiding new nanostructure design of N-coating metal-oxide-based electrodes. The possibility of nanoscale NiO promoting the reversible formation and decomposition of Li_2O_2 may inspire the study of the Li-O_2 cells.

Conflict of interest

The authors declare that they have no conflict of interest.

Acknowledgment

This work was supported by the NSF of China (Grant No. 51532002).

References

[1] J. Thomas, Lithium batteries: a spectacularly reactive cathode, Nat. Mater. 2 (2003) 705–706.
[2] K. Kang, Y.S. Meng, J. Bréger, et al., Electrodes with high power and high capacity for rechargeable lithium batteries, Science 311 (2006) 977–980.
[3] M. Armand, J.M. Tarascon, Building better batteries, Nature 451 (2008) 652–657.
[4] N. Kang, J.H. Park, J. Choi, et al., Nanoparticulate iron oxide tubes from microporous organic nanotubes as stable anode materials for lithium ion batteries, Angew. Chem. Int. Ed. 51 (2012) 6626–6630.
[5] J. Guo, Q. Liu, C. Wang, et al., Interdispersed amorphous MnO_x-carbon nanocomposites with superior electrochemical performance as lithium-storage material, Adv. Funct. Mater. 22 (2012) 803–811.
[6] M. Dirican, Y. Lu, Y. Ge, et al., Carbon-confined SnO_2-electrodeposited porous carbon nanofiber composite as high-capacity sodium-ion battery anode material, ACS Appl. Mater. Interfaces 7 (2015) 18387.
[7] H. Huang, T. Feng, Y. Gan, et al., TiC/NiO core/shell nanoarchitecture with battery-capacitive synchronous lithium storage for high-performance lithium-ion battery, ACS Appl. Mater. Interfaces 7 (2015) 11842.
[8] B. Xu, Y. Luo, T. Liu, et al., Ultrathin N-doped carbon-coated TiO_2 coaxial nanofibers as anodes for lithium ion batteries, J. Am. Ceram. Soc. (2017) 1–9.
[9] G. Tan, F. Wu, Y. Yuan, et al., Freestanding three-dimensional core–shell nanoarrays for lithium-ion battery anodes, Nat. Commun. 7 (2016) 11774.
[10] C. Wang, H. Wu, Z. Chen, et al., Self-healing chemistry enables the stable operation of silicon microparticle anodes for high-energy lithium-ion batteries, Nat. Chem. 5 (2013) 1042–1048.
[11] R. Raccichini, A. Varzi, V.S. Chakravadhanula, et al., Boosting the power performance of multilayer graphene as lithium-ion battery anode via unconventional doping with in-situ formed fe nanoparticles, Sci. Rep. 6 (2016) 23585.
[12] K. Fu, O. Yildiz, H. Bhanushali, et al., Aligned carbon nanotube-silicon sheets: a novel nano-architecture for flexible lithium ion battery electrodes, Adv. Mater. 25 (2013) 5109–5114.
[13] W.J. Zhang, A review of the electrochemical performance of alloy anodes for lithium-ion batteries, J. Power Sources. 196 (2011) 13–24.
[14] G.X. Wang, L. Sun, D.H. Bradhurst, et al., Nanocrystalline NiSi alloy as an anode material for lithium-ion batteries, J. Alloys Compd. 306 (2000) 249–252.
[15] M.T. McDowell, S.W. Lee, J.T. Harris, et al., In situ TEM of two-phase lithiation of amorphous silicon nanospheres, Nano Lett. 13 (2013) 758–764.
[16] H. Wu, G. Chan, J.W. Choi, et al., Stable cycling of double-walled silicon nanotube battery anodes through solid-electrolyte interphase control, Nat. Nanotechnol. 7 (2012) 310–315.
[17] H. Wu, G. Zheng, N. Liu, et al., Engineering empty space between Si nanoparticles for lithium-ion battery anodes, Nano Lett. 12 (2012) 904–909.
[18] X. Zhou, L.J. Wan, Y.G. Guo, Binding SnO_2 nanocrystals in nitrogen-doped graphene sheets as anode materials for lithium-ion batteries, Adv. Mater. 25 (2013) 2152–2157.
[19] Y. Gu, F. Wu, Y. Wang, Confined volume change in Sn-Co-C ternary tube-in-tube composites for high-capacity and long-life lithium storage, Adv. Funct. Mater. 23 (2013) 893–899.
[20] J. Zhang, A. Yu, Nanostructured transition metal oxides as advanced anodes for lithium-ion batteries, Sci. Bull. 60 (2015) 823–838.
[21] H. Wu, G. Chan, J.W. Choi, et al., Stable cycling of double-walled silicon nanotube battery anodes through solid-electrolyte interphase control, Nat. Nanotechnol. 7 (2012) 310–315.
[22] G. Evmenenko, T.T. Fister, D.B. Buchholz, et al., Morphological evolution of multilayer Ni/NiO thin film electrodes during lithiation, ACS Appl. Mater. Interfaces 8 (2016) 19979–19986.
[23] G. Kresse, J. Furthmüller, Efficient iterative schemes for ab initio total-energy calculations using a plane-wave basis set, Phys. Rev. B 54 (16) (1996) 11169.
[24] W. Kohn, L.J. Sham, Self-consistent equations including exchange and correlation effects, Phys. Rev. 140 (4A) (1965) A1133.
[25] P.E. Blöchl, Projector augmented-wave method, Phys. Rev. B 50 (24) (1994) 17953.
[26] G. Kresse, D. Joubert, From ultrasoft pseudopotentials to the projector augmented-wave method, Phys. Rev. B 59 (3) (1999) 1758.
[27] W.H. Shin, H.M. Jeong, B.G. Kim, et al., Nitrogen-doped multiwall carbon nanotubes for lithium storage with extremely high capacity, Nano Lett. 12 (2012) 2283–2288.
[28] Y. Huang, Z. Xu, J. Mai, et al., Revisiting the origin of cycling enhanced capacity of Fe_3O_4 based nanostructured electrode for lithium ion batteries, Nanomater, Nanomater. Energy 41 (2017).